SWEET BRIAR COLLEGE
3 2449 0446312 %

Digitized by the Internet Archive
in 2010 with funding from
Lyrasis Members and Sloan Foundation

http://www.archive.org/details/searchforemissio00neur

A Search for Emission from Variable and Transient Radio Sources Near the Galactic Center

A Senior Honors Thesis in the Department of Physics, Sweet Briar College

by Jennifer Neureuther

Defended and Approved 10 April 2003

Scott D. Hyman 2003 April 21

Dr. Scott Hyman date

2003 April 21

Dr. Joseph Lazio date

2003 April 21

Dr. Grant Denn date

To my parents for their strength and support, Dr. Hyman for his endless encouragement, and Margaret Sullivan for reminding me of the meaning of it all.

Special thanks to Joseph Lazio, Namir Kassim, and Mike Nord of
The Naval Research Laboratory for their collaboration.

A Search for Emission from Variable and Transient Radio Sources Near the Galactic Center

Honors Thesis

Jennifer Neureuther
Class of 2003
Sweet Briar College

Advisor:
Dr. Scott Hyman
Associate Professor
Sweet Briar College

Abstract

We report on a 330 MHz survey of small-diameter radio sources in a $4° \times 4°$ field of view centered on the Galactic center. On three six-hour observations made during October 1996, March 1998, and September 1998, 147 sources were measured and compared. An additional subset of 126 sources were also measured on an image created from one-hour observations made between March and July 2002. The sources were systematically evaluated for variability, revealing no new variables. Similarly, a search for transients revealed only two already documented by our group. We report the occurrence of transients brighter than 75 mJy and with timescales six hours or longer in the Galactic center region to be no less than 46 $(°)^{-2}\, yr^{-1}$.

Chapter 1 Introduction

The existence of galaxies was proven in 1924 and since then many varieties of these huge collections of stars have been classified. The majority of galaxies observed thus far fall into one of three categories: *elliptical*, *spiral*, or *irregular*. Our own galaxy is a spiral galaxy identifiable as a relatively thin disc with spiral arms (Figure 1). Spiral galaxies are further classified in to subgroups depending on how many arms they have and the spacing of those arms. All spiral galaxies contain between 10^6 and 10^{12} stars, and have a dense central region.

Figure 1. Example of a Spiral Galaxy (NGC4414)[1]

The center of our Galaxy remained relatively unexplored by astronomers until well into the twentieh century. From our location, two-thirds of the way from the center

[1] Hubble Space Telescope 1999 hubble.stsci.edu

to the outer edge of the disk, intervening gas and dust as well as confusing bright sources make observations of the center of our Galaxy particularly difficult and imprecise. When making observations of the Galactic center, emission of electromagnetic radiation in the radio spectrum ($0.01\text{m} < \lambda < 10\text{m}$) is of particular interest to astronomers. These relatively low-energy waves can be observed from earth, unlike the high-energy x-ray spectrum ($\lambda \sim 5\times10^{-11}\,\text{m}$), which is absorbed by Earth's protective atmosphere.

Karl Jansky made the first observation of extragalactic sources of radio emission in 1933 (Jansky, 1935). Working for Bell Labs to investigate possible sources of static, Jansky detected a faint but constant radio source that rose and set in the sky every day. He monitored the source using a simple wire antenna, and he eventually determined that radio waves were coming from the direction of the center of the Galaxy. Bell Labs, however, was no longer concerned with the source of the emissions since they did not interfere with short wave communication and gave Jansky a different project. Years later the basic unit of flux per wavelength, $10^{-26}\,\frac{W}{m^2 Hz}$, was defined as a Jansky.

Figure 2. Reconstruction of Karl Jansky's Radio Telescope. Green Bank, West Virginia[2]

Though Janksy's discovery was published in an engineering journal, few astronomers thought radio emissions of the universe were scientifically significant and continued to focus on optical observations. Grote Reber, an engineer who mass-produced radios, learned of Jansky's work and saw the potential wealth of information that radio observations offered. He built a radio telescope and recorded the first systematic survey of radio emission by scanning his receiver across the sky at night when there was little radio interference form manmade sources (Figure 3). Reber's early work, which covered more than a decade, was published in both astronomy and engineering journals drawing the attention of quite a few astronomers.

[2] www.draco.scsu.edu

Figure 3. Reber's Radio Telescope[4]

After World War II, institutions eager to follow up on Reber's surveys hired many engineers who had been trained by the military to send and receive radio signals as well as maintain radio equipment. Often using surplus army radio receivers, new observations were made at several radio wavelengths. To improve the observations, larger antennas were built to make higher resolution and higher sensitivity maps of the radio sky. Radio telescopes such as The Very Large Array (VLA), and The Very Long Baseline Array (VLBA), have been used to achieve very high resolutions, and currently

the highest resolutions have been achieved through Very Long Baseline Interferometry (VLBI).

The appeal of radio observations over optical observations is due to the fact that radio emissions are not affected as much by interstellar dust, as is optical light. The radio wavelengths are on a much larger scale than particles, therefore gas and dust surrounding the Galactic center has a much less adverse effect on radio observations. Even with this advantage, the first radio surveys found the high-density Galactic center region to be difficult to observe and map. Most recently, developments in radio interferometry and data reduction techniques have made it possible to study our Galactic center and the many structures therein with unprecedented detail.

LaRosa et al. (2000) published an image of the Galactic center synthesized from low frequency (330 MHz), wide-field VLA radio observations made in 1989 (Figure 4). The image covers an area of the sky four degrees square and the variety, intensity range, and detail of the objects seen in the image is clear. Note the presence of star formation regions (HII regions) and hot synchrotron emitting plasma from exploded stars (supernova remnants--SNRs) as well as a range of SNR sizes, which is indicative of their different ages. At the very center of the area denoted as Sgr A, astronomers have discovered evidence of a supermassive black hole, an object with a mass $\geq 10^6 M_\Theta$ which may be responsible for the enormous activity surrounding it. The long thin filamentary sources are thought to trace the magnetic field lines at the Galactic center (Morris & Yusef-Zadeh 1985; Bally & Yusef-Zadeh 1989; Gray et al 1991; Anantharamaiah et. al. 1991). Recent developments in the imaging and analysis of these filaments has led to the

hypothesis that the magnetic field of the galactic center is not as uniform as was once believed.

Figure 4. Wide-Field Galactic Center Image

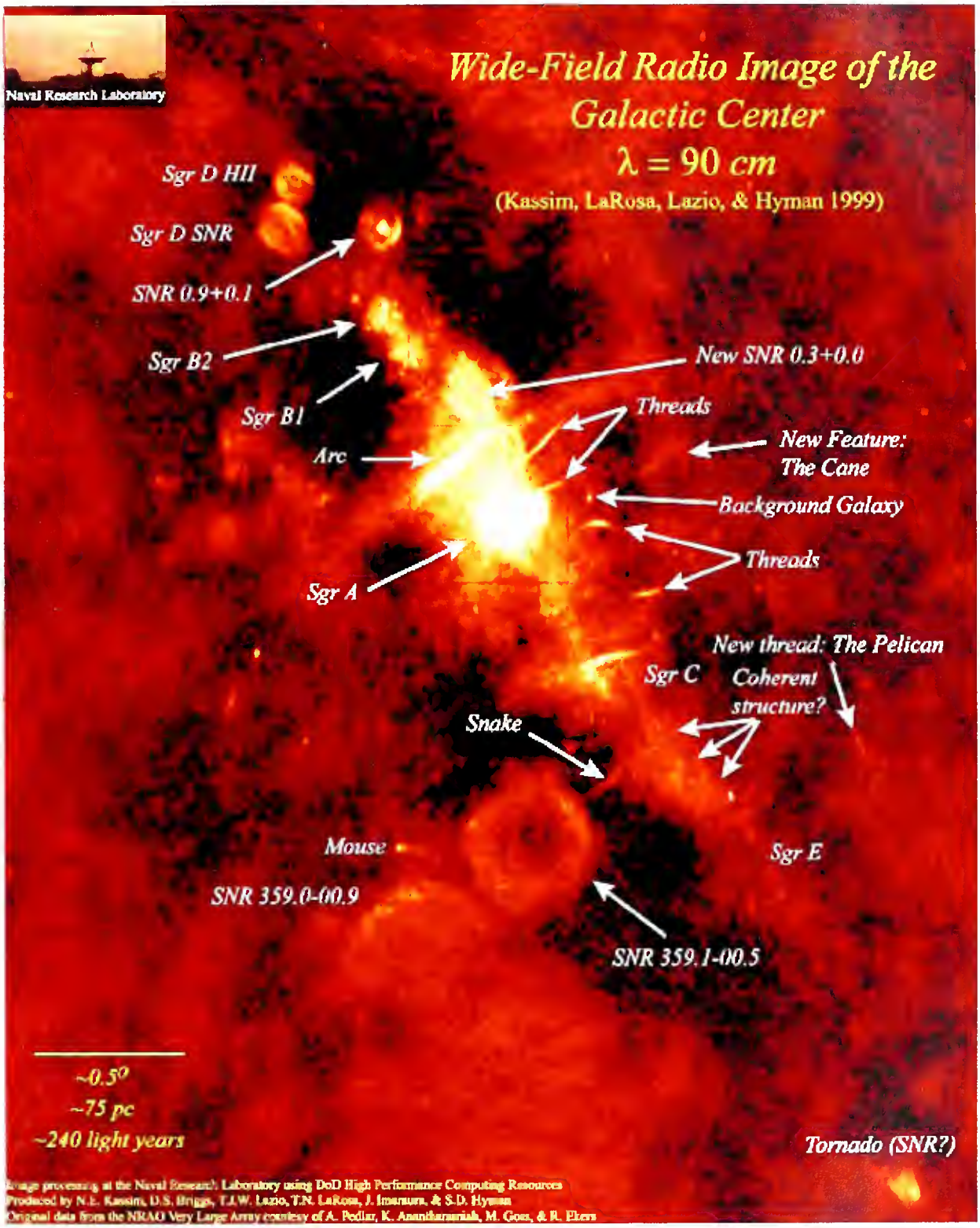

In addition to the extended bright structures seen in Figure 2, there are hundreds of point sources in the Galactic center. A representative field of these is shown in Figure 5. These sources are fascinating objects such as background galaxies, HII regions, pulsars, and supernova remnants. Of particular interest are *transient* and *variable* sources, which are, respectively, objects that significantly brighten and then fade forever, and those whose intensities brighten and fade more than once. Some of these sources may be black hole or neutron star binary systems that will be described further in Chapter 2.

Figure 5. Field of point sources in the Galactic center.

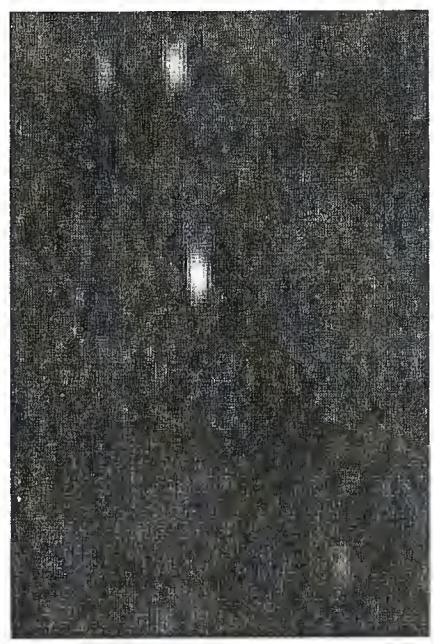

This project explores the abundance and individual properties of transient and variable sources in the area of the center of our Galaxy. While transients have been

found in radio observations of the entire Galactic plane, this is the first systematic monitoring program of the transient and variable sources in the Galactic center. Since stellar density increases toward the Galactic center we expect a larger density of transient objects in this region.

The scattering of light by gas and dust in our atmosphere causes the twinkling or *scintillation* of optical stars when viewed from earth. The stars appear momentarily broader with changes in the density of the earth's atmosphere. We might worry about this same effect on Galactic center sources when very large clouds of gas and dust pass in front of the sources. Assuming a source to be in the Galactic center about 8,000 parsecs distant and the cloud of gas and dust to be moving at $100 Km \cdot s^{-1}$, a typical speed of objects in the Galactic center, even a small scintillation of 1" would take place over tens of thousands of years from our view point on earth. Therefore any variability we detect is not due to scintillation.

One of the first radio transients was detected in 1976 by observers at the Nuffeild Radio Astronomy Laboratories, and was found to emit X-ray radiation as well as radio (Davies et al). One significantly high flux density measurement in radio and x-ray emission was observed out of about seven measurements over the course of a year of monitoring for this source.

Many X-ray transients have been found in the last few decades elsewhere in our galaxy, but far fewer have been detected in the radio, due to previous sensitivity and resolution limitations. In the last ten years, the VLA has been substantially upgraded to enable low frequency observations that do not suffer from these limitations.

In 1990 a transient radio source was detected and confirmed to be located in the Galactic center (Zhao et al). It was observed to have a timescale of about three months. In 1998 a group studying an X-ray transient in the Galactic center found transient radio emission as well with a timescale of one month to one year. (Hjellming et al). Hyman et al (2000) detected low frequency radio emission from this transient, and also found another unusual radio transient that apparently had no corresponding X-ray emission and a faster timescale of a month at most.

In this project, four observations of the Galactic center made during the last six years were compared in order to detect variable and transient sources. Initially 103 sources were found with a search by eye on two of the maps. Then using a list of Galactic center radio sources exactly 147 sources were detected on images made from three observations, and a subset of 126 sources were measured on a map made from the fourth observation. These measurements were then checked for variables and transients. Chapter 2 presents the theory behind variable and transient radio emission, and the basics of radio observations. Chapter 3 describes the techniques used to detect and measure the radio sources, and in Chapter 4 we summarize the results and future direction of this project.

Chapter 2 Theory

a. Stellar Evolution and The Origin of Transient Events

Star formation begins with the gravitational attraction of neutral hydrogen atoms into a dense region. Eventually the region becomes sufficiently dense and hot for the fusion of hydrogen into helium to take place. A helium core is gradually created, and in stars of significant mass the core becomes sufficiently dense and hot for fusion of helium into carbon to take place. A large amount of energy produced by the helium fusion causes the star to expand and become a Red Giant.[3] Figure 6 illustrates this evolution.

Figure 6. Evolution of Star to Red Giant

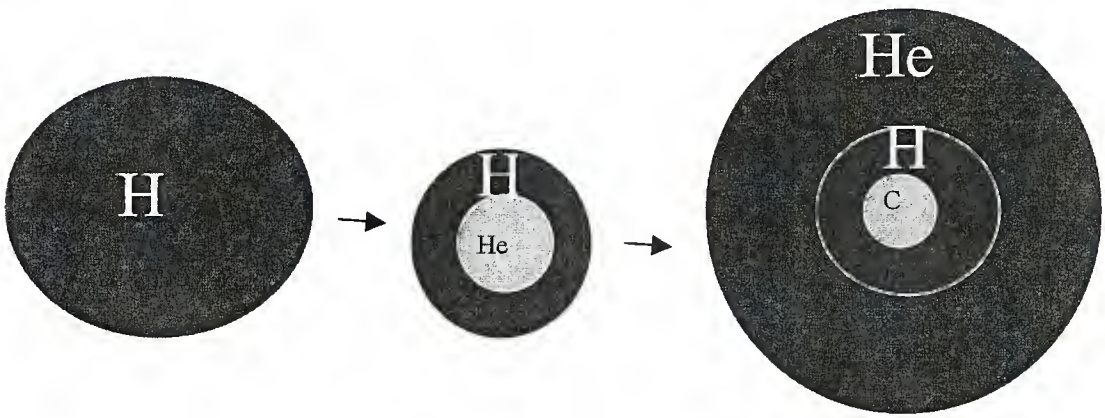

Most stars will not evolve beyond the Red Giant stage, however those with masses greater than eight times that of our sun will proceed with the fusion of heavier and heavier elements in their cores. The most massive stars will eventually achieve the fusion of silicon and sulfur creating an iron core. For the iron core to undergo fusion,

unlike the previous elements which all output energy that supports the outer layers the star, energy is required. This causes the star to rapidly collapse and creates a supernova explosion, which ejects the outer layers of the star. What remains of the star is one of two extremely dense objects, either a black hole with a density around $10^{19}\ kg/m^3$ and Schwarzschild radius of a few kilometers, or a neutron star, with density $\approx 4\times10^{16}\ kg/m^3$ and radius $\approx 10km$ (Zeilik). Neutron stars are stellar remnants with mass, m, $1.4M_{\Theta} \le m \le 3.0M_{\Theta}$. Rapidly rotating neutron stars with strong magnetic fields are called pulsars, because of the rotationally synchronized radio emission. Black holes are at least 3.0 times the mass of our sun, and have an escape velocity greater than the speed of light, thus trapping all light and giving the "black" appearance.

Transient and variable sources are believed to arise in binary star systems that consist of a red giant and a black hole or neutron star, which gravitationally draw in and sweep up the ejected outer layers of the normal star. These objects are so dense that the gas is gravitationally drawn in to form an *accretion disk* around the black hole or neutron star. The accretion disk heats up to very high temperatures leading to emission of X-rays, and occasionally extremely powerful X-ray outbursts. Accompanying these X-ray transient events are radio bursts of synchrotron radiation arising from high-energy electrons spiraling around the very strong magnetic fields present near the poles of the black hole or neutron star (Figure 7). The events described take place in different magnitudes for black holes and neutron stars; therefore when a transient is found it can be determined to be either a black hole or neutron star based on the ratio of its radio to X-ray

[3] http://observe.arc.nasa.org

emissions. Fender et al (2001) found that suspected black holes will have a significantly higher ratio of peak radio emission to peak x-ray emission than neutron stars.

Figure 7. Artist's rendition of a neutron star or black hole binary system[4].

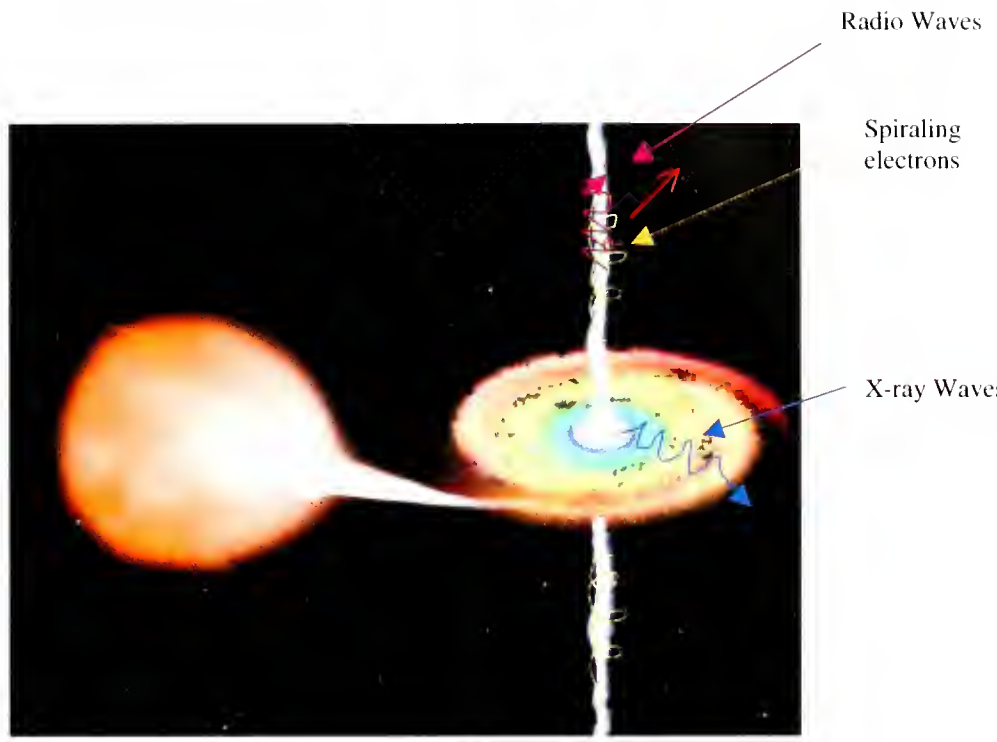

b. The VLA and Interferometry

To collect emission from radio sources at various wavelengths a parabolic reflecting dish antenna is used to focus the emission to a central receiver (Figure 8). As a simple example, consider a point source located very distant from the antenna. The image of the source, a *point spread function,* resembles a single slit diffraction pattern (Figure 9) where the central peak corresponds to the source location. The resolution, r, of the

antenna is $r \propto \frac{\lambda}{D}$, where λ is the wavelength observed and D is the diameter of the dish.

The highest resolution currently available for a single dish is that of Arecibo in Puerto Rico which offers a resolution of 3.5' at the wavelength of 20 cm[5].

Figure 8. Single dish antenna receiver.

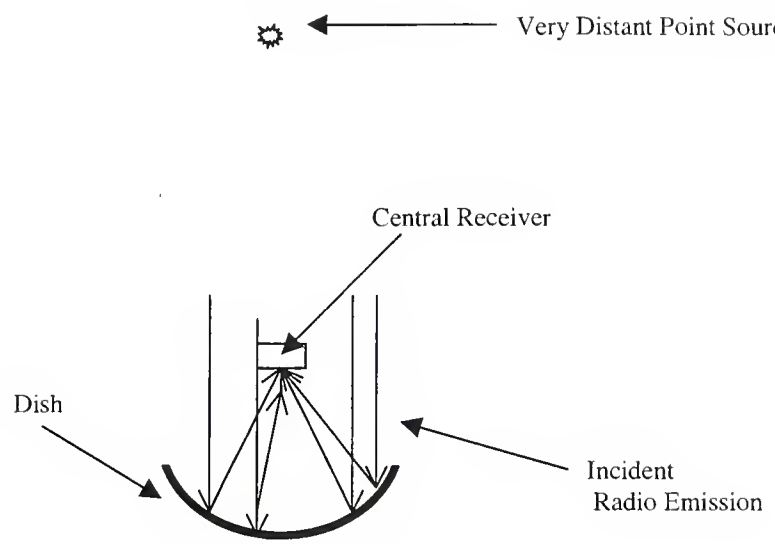

Figure 9. Single slit diffraction pattern[6]

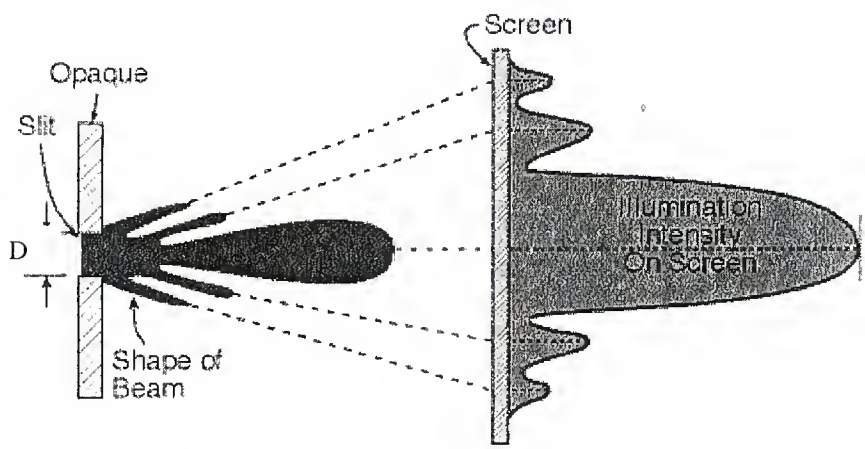

[4] NASA Press Release 10/2002
[5] www.naic.edu

Instead of building larger antennas to achieve higher resolutions, arrangements of several smaller antennas working together as an *interferometer* can be used to simulate one large antenna. Using an array of antennas saves time and money compared to the construction of one large antenna. For interferometers, the resolution is related to wavelength as: $r \propto \frac{\lambda}{d}$, where d is the diameter of the array. Moving the positions of the dishes can provide for effectively much larger antennas of varying resolutions.

Observations from interferometers consist of the correlated signals, called *visibilities,* observed from each pair of antennas, or *baselines.* A single visibility yields an image with intensity varying sinusoidaly in a manner similar to a double slit interference pattern. The actual radio image is synthesized by combining the visibilities detected for each pair of antennas. The combination of all visibilities for all baselines results in an image where constructive interference occurs at the location of the real sources and destructive inference occurs everywhere else. That image is referred to as the *dirty image*, because the effects of the point spread function or *synthesized beam pattern* of the entire array have not yet been compensated for on the image.

Once the dirty image is made, the beam pattern must be deconvolved from the dirty image to yield the real image in a process called "cleaning". The image must also be *primary beam* corrected for the point spread function of the individual antenna (See Figure 9), which otherwise decreases the sensitivity, s, of an array of the image the further away from the center a source is located. The sensitivity is a measure of electronic noise that becomes smaller with increasing individual dish size.

---

[6] www.ksu.edu

While an interferometer has the resolution of the larger effective dish, it only has the sensitivity of the total collecting area of its single dishes. Sensitivity also varies with time as $s \propto \frac{1}{\sqrt{t}}$, where t is the duration of the observation, thus longer observations have better sensitivity. The National Radio Astronomy Observatory operates the Very Large Array (VLA) in New Mexico, which uses interferometry to combine twenty-seven 25-meter diameter antennas into effectively one giant dish. The antennas are arranged in a "Y" formation (Figure 10) and placed on tracks so that they may be moved to simulate single dish antennas of different sizes. VLA makes observations in four main configurations. These configurations are named by letters A through D, and range in size from an effective diameter of 36 kilometers (A configuration) to 1 kilometer (D configuration), respectively. In A configuration the VLA offers a resolution at 20 cm wavelength of 1.4" and at 90 cm, the wavelength for this project, of 6". Table 1 shows the details of the observations taken at the VLA that were used in this research.

Figure 10. Very Large Array (Socorro, New Mexico)

Table1. Observation details

Configuration/ Observation Date	Resolution	Duration (hours)	Sensitiviyty, rms mJy/bm
A/ October 1996	11.43" x 6.61"	5.5	~3
A/ March 1998	9.62" x 5.07"	6.7	~3
B/ September 1998	32.48" x 16.45"	6.7	~3
AB/ March-July 2002	14.36" x 8.17"	6	~3

The different resolutions lead to differences in source measurements from map to map. Figure 11 shows an example of a large source imaged in configuration B and the same source which appears much fainter in a map made from data taken in configuration A. The lower resolution B map offers more comprehensive images of extended structure while such sources may be resolved out on A due to the higher resolution. For example in Figure 11 the peak to noise ratio for the source on map A is 9.2 while on map B it is 14.1. This measurement difference can be caused by one of two resolution issues. Either the source has some extend areas that are not picked up on A and thus is measured too low on A or the source is near some extended structure that only appears on B and is measured with it making the B measurement too high. Whether or not the extended structure is actually a part of the source is hard to determine. This resolution discrepancy will be taken into account when we make our comparisons in the search for variables and transients.

Figure 11. Extended point source

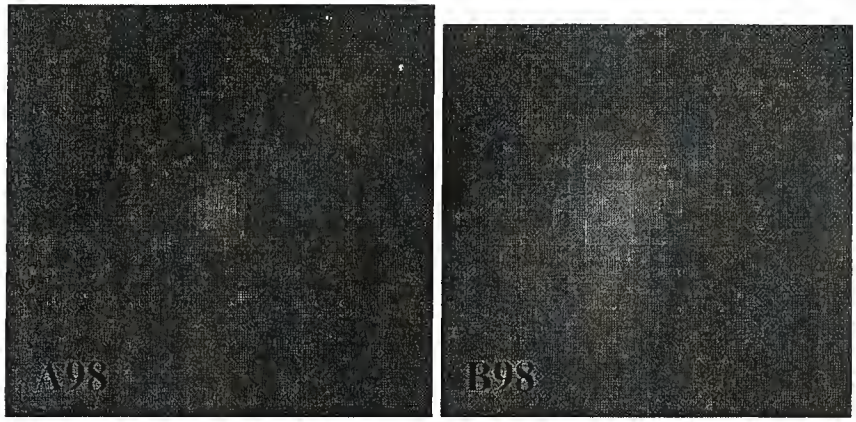

The imaging and analysis of the radio observations was accomplished with the Astronomical Image Processing System (AIPS), which is the standard software available from the National Radio Astronomy Observatory.

Chapter 3 Source Measurement

a. Algorithms for Measuring

The first task in measuring the sources was to identify the locations of the sources and set a guideline to distinguish real sources from image artifacts. Initially the search was done by scanning the image by eye for areas that appear brighter, indicating a higher flux density. The first comparison was between two maps made from the observations in 1998; one in A configuration (A98) and one in B configuration (B98). A source list was established which aided in the search on maps made from observations in A configuration in 1996 (A96) and from a mixture of A and B configuration observations in 2002 (AB02).

Sources were measured in two different ways. In the first, the average background emission, b, and the standard deviation, σ , was estimated by sampling around the source using the AIPS task TVSTAT. The task IMSTAT was then used to measure the mean flux density, <I>, of the source. The integrated flux density, S, was then calculated as: $S = (< I > -b) \times N$, where N is the size of the source in beams. Uncertainty in this flux was calculated as: $\Delta S = \sqrt{N} \times b_{rms}$, where b_{rms} is the root-mean- square uncertainty about the mean background flux density level. In the second method, the task IMFIT was used to fit a two-dimensional Gaussian brightness distribution, $I(x, y)$, and background level to the source,

$$I(x, y) = Ae^{-(x-\bar{x})^2/(2\sigma_x^2)} e^{-(y-\bar{y})^2/(2\sigma_y^2)} + B ,$$

where A is the peak intensity, B is the background level and $\bar{x}$ and $\bar{y}$ are the coordinates of the peak position. In addition to the fitted peak intensity, A, IMFIT derived the integrated intensity, S, and the uncertainty in each.

The A configuration images were synthesized from hundreds of smaller fields to account for the curvature of the sky; otherwise sources would have been significantly distorted. Each separate field was searched for all compact sources, applying the criteria that their intensities be greater than $5\sigma + B$, but also requiring that the source be larger than nine pixels in size in order to eliminate small-sized artifacts, which inevitably result from imperfect image processing. Approximately 10 sources were eliminated on each map by these criteria. A similar method was used to measure all sources on the B98 map, which was synthesized from 55 fields.

The individual fields overlap, so some of the sources were measured two to four times. These multiple measurements were found to agree to within 10% of each other, giving us confidence that the imaging and measuring techniques were sound to 10% and that one could measure off one larger image created by combining individual fields. Thirteen pairs of very close together sources called doubles, and sources that otherwise appeared extended were not measured because their inconsistencies between configurations would confound the search for variable and transient sources. This resulted in a list of 103 sources that were measured on both maps.

b. Comparing Epochs

A master list of sources in the Galactic center was compiled by one of our collaborators, Mike Nord, at the Naval Research Laboratory. He compiled a list of 244

sources detected by applying the automated program Search and Destroy (SAD), that uses IMFIT to measure on a single map synthesized from the combination of the three observations in 1996 and 1998 (Nord et. al.). The fact that the map was synthesized from all of those epochs meant it had a very low noise level, and a great many weaker sources could be found that were not visible on the individual epoch images.

In an attempt to quickly measure the sources of Mike's list that were not in the database of 103 already measured, SAD was used to make measurements on the individual A98 and B98. However it was found that when plotting a sample of B98 flux densities vs. A98 flux densities for 72 sources, measurements made by SAD consistently had slightly more scatter (See figure 12) than those measurements made by individual IMFIT measurements seen in (See Figure 13). The uncertainty of the slope in Figure 13 is 5% and in Figure 14 is 3%. We believe that the larger scatter found in SAD measurements was due to errors the task made in choosing window sizes to place around the sources when fitting their parameters with IMFIT. SAD also included far too many noise artifacts, which were not real sources and it was difficult to sort out these measurements from actual sources. SAD was abandoned and the sources were measured by locating their coordinates directly.

Figure 12. SAD98 vs. SAD96 (72 sources)

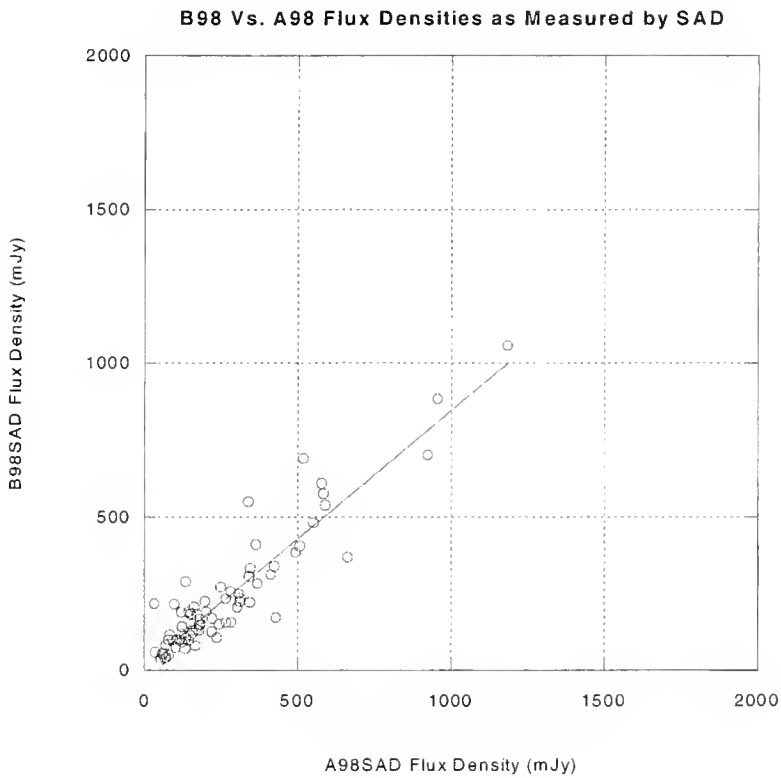

Figure 13. B98 vs.A98 by eye (72 Sources) (Not SAD)

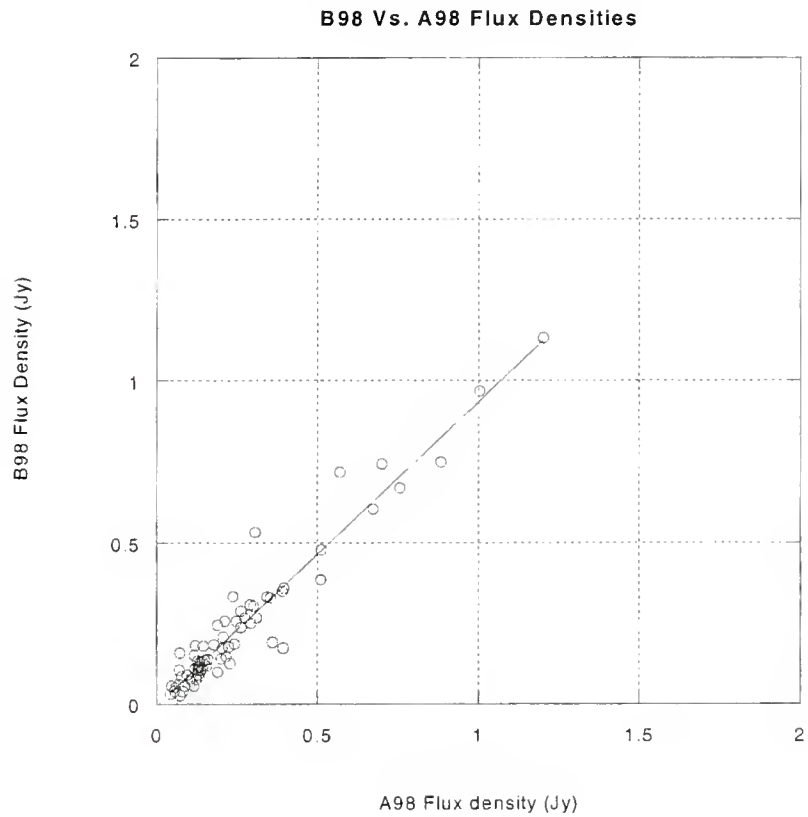

A great number of the 244 sources were not measurable on one or more of the individual epochs because the noise levels were almost twice as high compared to the combined map. Also approximately 12 sources were excluded because they were located outside the borders of the smaller maps or were doubles. The number of sources found and identified using Mike's coordinates on each epoch are listed in Table 2. The end result of searching and measuring was 147 sources that were measured on each of the

A98, B98, and A96 maps, as well as a sub set of 126 of the 147 that were measured on AB02.

Table 2. Number of Sources Measured.

Epoch	Number of sources measured
A98	184
B98	196
A96	177
AB02	126

Once all sources had been measured, the process of comparing measurements was initiated with the goal of finding sources that appeared either on only one map or more strongly on one than the other. This search was complicated by the fact that the data were taken while the antennas were in different configurations. For example, the A98 map had a higher resolution than the B98 map, which meant that larger, blurry or less defined sources would show up brighter in the B98 image, but only weakly on the A98 image (See Figure 11). Therefore, as a preliminary step the data sets were compared for overall agreement with the A98 data set and a correction was made so that the integrated flux densities of the sources were consistent overall. As seen in Figures 14 and 15, the source measurements differ overall only by a common factor that was then applied to the measurements for accurate comparison (Table 3). The A96 and AB02 maps had a slope less than one when those intensities were plotted against the A98 intensities; meaning sources were low by a common factor. The measurements from the B98 were also low

although not as much as A96 and AB02 compared to A98. The discrepancies between maps can be attributed to calibration errors.

Table 3. Correction Factors compared to A98

MAP	Correction Factor
B98	1.14
A96	1.21
AB02	1.21

Figure 14. B98 source Flux Density vs. A98 source Flux Density (161 Sources)

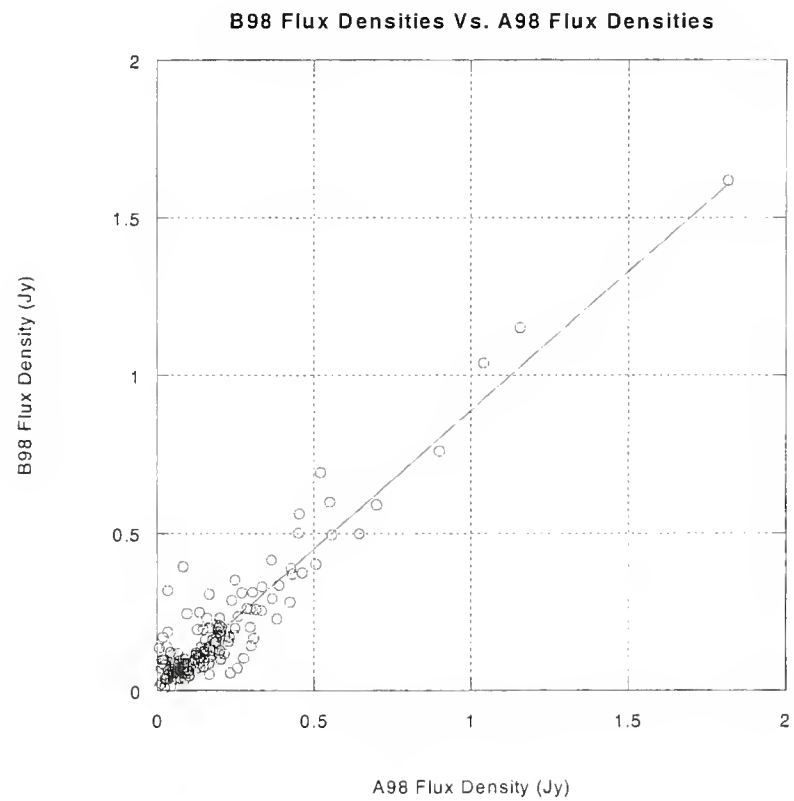

Figure 15. A96 source Intensities vs. A98 source Intensities (170 sources)

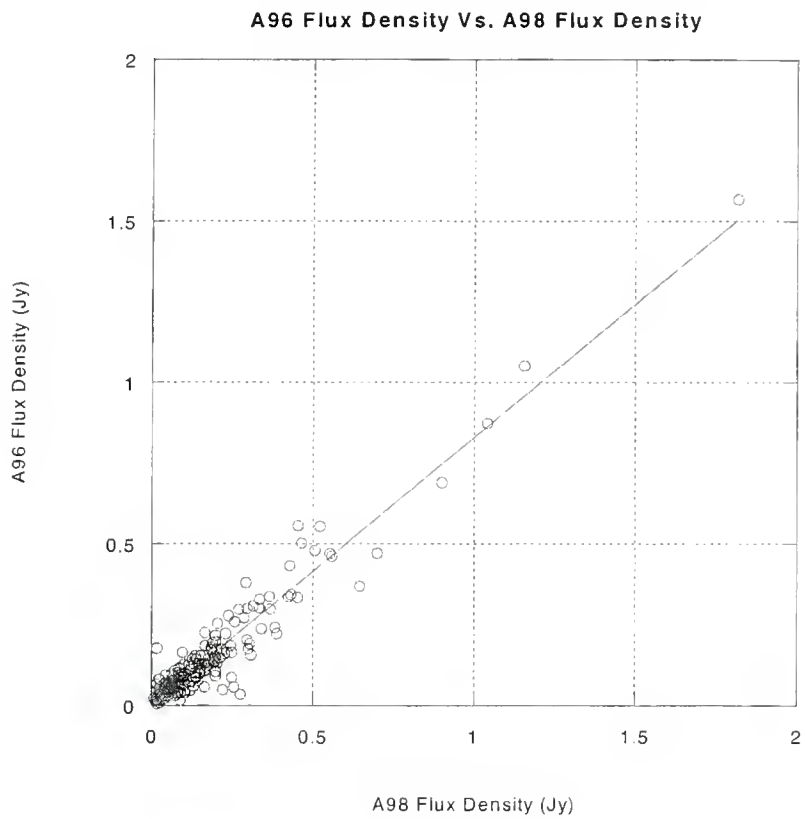

The 2002 data were taken at the VLA over a series of months from March to July. The intent of this was to compare the individual month images in order to look for transients or variables with time scales of around a month. We combined the data with the task DBCON in AIPS and after imaging, of the 147 sources, 126 were detected and measured on that map. This gave us a fourth epoch to check for variable and transient sources. The '02 source measurements were also checked for correspondence with A98 by graphing the source intensities. Once again in Figure 16 we see that the data needs

only to be corrected by a factor of 1.21 in order to accurately compare source measurements to other epochs.

Figure 16. AB02 source Intensities vs. A98 source Intensities (126 sources)

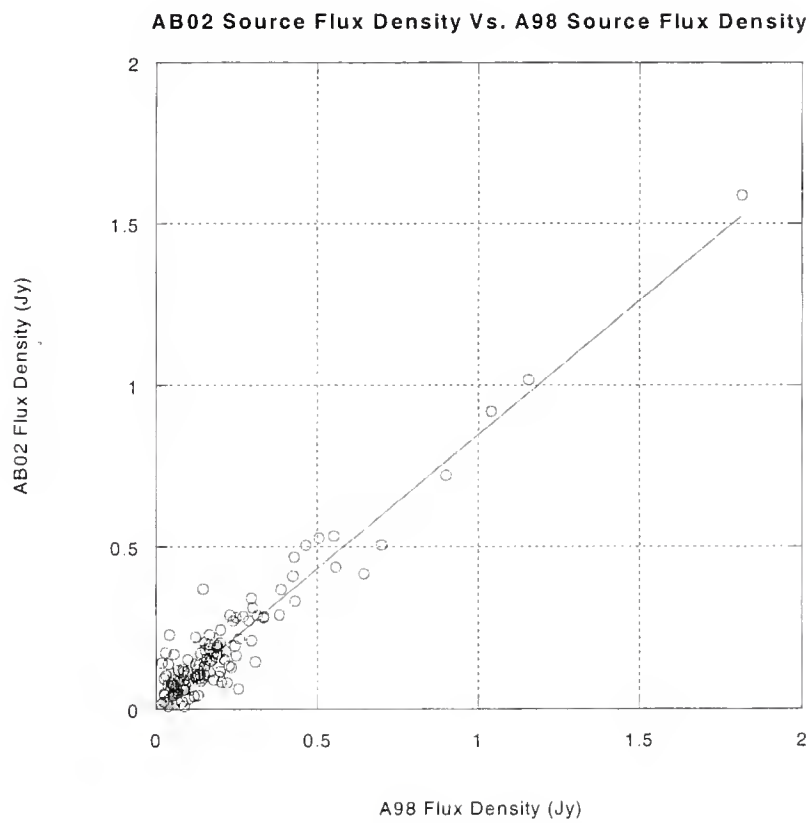

b. Variable Search Criteria and Methods

To search for variability, the corrected flux values for the A96, B98, and AB02 sources were respectively subtracted from the A98 measurements. Then the errors in these differences were found and a ratio, R, made of the difference to the error as follows:

$$R = \frac{S_1 - S_2}{\sqrt{(\Delta S_1)^2 + (\Delta S_2)^2}}$$

where S_i is the flux density of the sources on image i. Sources with $R \geq 5$ were considered to be good variable candidates and investigated further by remeasuring them and taking new measurements on maps from epochs other than the four being directly used for this project. Some sources whose ratios were three or larger were also investigated in hopes of catching something variable, but perhaps not that dramatic. All sources with ratios larger than three are listed the following tables.

Table 4. B98 to A98 Variable Candidates

Position (J2000) RA			DEC			A98 Flux (Jy)	ΔS	B98 Flux (Jy)	ΔS	R
17	49	7.24	-29	23	36.04	0.520	0.016	0.790	0.011	-13.8
17	47	20.16	-28	23	3.75	0.165	0.016	0.752	0.077	-7.41
17	50	12.25	-28	53	41.33	0.034	0.018	0.210	0.023	-5.98
17	47	6.21	-28	35	7.57	0.165	0.017	0.349	0.027	-5.72
17	49	8.44	-30	27	20.01	0.221	0.057	1.034	0.138	-5.44
17	50	0.29	-27	54	0.68	0.031	0.016	0.159	0.019	-5.09
17	48	1.07	-28	16	3.46	0.008	0.007	0.153	0.029	-4.94
17	44	37.12	-28	57	6.23	0.453	0.036	0.641	0.023	-4.38
17	44	59.7	-29	28	47.11	0.016	0.007	0.109	0.021	-4.27
17	43	44.55	-29	40	17.71	0.018	0.010	0.191	0.040	-4.15
17	39	30.38	-28	43	38.03	0.136	0.022	0.282	0.031	-3.91
17	46	51.61	-29	22	12.34	0.017	0.009	0.098	0.021	-3.61
17	48	15.59	-30	56	14.04	0.127	0.056	0.610	0.125	-3.52
17	40	41.61	-28	48	8.31	0.239	0.020	0.327	0.015	-3.49
17	52	58.7	-28	6	36.98	1.156	0.035	1.311	0.030	-3.39
17	45	13.92	-29	29	24.8	0.033	0.010	0.362	0.098	-3.32
17	52	22.73	-28	37	36.23	1.041	0.028	1.183	0.033	-3.28
17	44	59.39	-29	16	0.73	0.019	0.009	0.110	0.028	-3.07
17	38	16.17	-28	52	28.34	0.043	0.017	0.138	0.026	-3.04
17	43	50.55	-29	37	12.53	0.256	0.052	0.081	0.016	3.20

Table 5. A96 to A98 Variable Candidates

Position (J2000) RA			DEC			A98 Flux (Jy)	ΔS	A96 Flux (Jy)	ΔS	R
17	50	0.29	-27	54	0.68	0.031	0.016	0.564	0.092	-5.71
17	49	7.24	-29	23	36.04	0.520	0.016	0.669	0.021	-5.63
17	39	12.69	-28	46	58.48	0.292	0.021	0.459	0.024	-5.25
17	44	37.12	-28	57	6.23	0.453	0.036	0.671	0.025	-4.95
17	40	41.61	-28	48	8.31	0.239	0.020	0.337	0.020	-3.46
17	39	37.92	-28	33	42.3	0.206	0.016	0.307	0.028	-3.10
17	43	5.45	-27	36	2.61	0.506	0.017	0.581	0.017	-3.09
17	47	6.21	-28	35	7.57	0.165	0.017	0.272	0.031	-3.03
17	42	28.07	-28	2	8.24	0.316	0.013	0.372	0.014	-3.01
17	42	54.49	-30	7	6.28	0.276	0.073	0.041	0.017	3.12
17	43	50.55	-29	37	12.53	0.256	0.052	0.069	0.014	3.45

Table 6. AB02 to A98 Variable Candidates

Position (J2000) RA			DEC			A98 Flux (Jy)	ΔS	AB02 Flux (Jy)	ΔS	R
17	44	59.39	-29	16	0.73	0.019	0.009	0.172	0.029	-5.05
17	43	5.45	-27	36	2.61	0.506	0.017	0.638	0.023	-4.54
17	51	6.73	-30	22	15.1	0.146	0.036	0.446	0.056	-4.49
17	38	16.17	-28	52	28.34	0.043	0.017	0.277	0.056	-3.98
17	49	14.6	-28	15	37.12	0.031	0.011	0.123	0.021	-3.88
17	43	5.48	-27	49	26.86	0.200	0.018	0.294	0.021	-3.46
17	50	0.29	-27	54	0.68	0.031	0.016	0.208	0.049	-3.42
17	42	48.49	-28	25	21.76	0.071	0.015	0.144	0.016	-3.39
17	42	44.02	-29	49	13.33	1.816	0.025	1.920	0.022	-3.17
17	47	6.21	-28	35	7.57	0.165	0.017	0.238	0.016	-3.11
17	43	50.55	-29	37	12.53	0.256	0.052	0.075	0.015	3.32

The R values for the sources listed in the tables are almost all negative. This reflects the fact that most of the high ratio sources found were ultimately explainable by resolution differences. B98 has lower resolution than A98 so we expect B98 to yield higher flux measurements for extended sources, leading to negative R values. Similarly the AB02 data was a mixture of A and B configurations and had a lower resolution than a pure A map and the majority of its R values were negative. Finally examining the A96 map, we see from Table 1 that it too has lower resolution than A98.

A comparison was also made between AB02 and A96 as well as A96 and B98 to look for sources with unusually high R-values that are not already on the previous tables. The intensities were plotted against each other, the correction factor found, and R calculated. The resulting R values can be found in Tables 7 and 8.

Table 7. AB02 to A96 Variable Candidates (corrected values)

Position (J2000) RA			DEC			A96 Flux	ΔS	AB02 Flux	ΔS	R
17	44	59.39	-29	16	0.73	0.017	0.010	0.171	0.029	-5.06
17	51	6.73	-30	22	15.1	0.152	0.042	0.444	0.056	-4.17
17	49	9.8	-30	45	5.05	0.263	0.028	0.442	0.035	-4.01
17	49	14.6	-28	15	37.12	0.032	0.013	0.123	0.021	-3.69
17	41	11.14	-27	35	15.93	0.089	0.022	0.266	0.045	-3.51
17	54	12.79	-28	54	16.38	0.126	0.033	0.274	0.029	-3.37
17	38	16.17	-28	52	28.34	0.082	0.026	0.276	0.056	-3.15
17	50	0.29	-27	54	0.68	0.550	0.090	0.207	0.049	3.35

Table 8. B98 to A96 Variable Candidates (corrected values)

Position (J2000) RA			DEC			A96 Flux	ΔS	B98 Flux	ΔS	R
17	49	8.44	-30	27	20.01	0.056	0.016	1.025	0.137	-7.04
17	47	20.16	-28	23	3.75	0.217	0.027	0.745	0.077	-6.48
17	44	10.84	-29	25	55.17	0.077	0.019	0.595	0.079	-6.33
17	49	7.24	-29	23	36.04	0.652	0.020	0.783	0.011	-5.61
17	36	35.95	-29	0	5.39	0.102	0.032	0.395	0.046	-5.26
17	43	44.55	-29	40	17.71	0.008	0.005	0.190	0.040	-4.52
17	36	5.4	-28	32	28.07	0.395	0.033	0.565	0.033	-3.63
17	52	22.73	-28	37	36.23	1.030	0.023	1.173	0.033	-3.58
17	48	15.59	-30	56	14.04	0.169	0.046	0.604	0.124	-3.29
17	44	59.39	-29	16	0.73	0.017	0.010	0.109	0.028	-3.10
17	42	54.49	-30	7	6.28	0.040	0.017	0.115	0.018	-3.01
17	40	0.6	-27	48	15.36	0.592	0.042	0.424	0.030	3.28
17	41	37.75	-28	4	36.96	0.354	0.016	0.285	0.013	3.35
17	42	28.07	-28	2	8.24	0.363	0.014	0.292	0.016	3.38
17	41	49.6	-29	44	59.72	0.149	0.012	0.090	0.010	3.70
17	43	5.45	-27	36	2.61	0.566	0.016	0.455	0.022	4.07
17	50	0.29	-27	54	0.68	0.550	0.090	0.157	0.019	4.27

A histogram of the ratio $\frac{S_{1,2} - S_{avg}}{S_{avg}}$ was made for a comparison between A98 and A96 (Figure 17) where S_1 is the A98 source flux density, S_2 is the A96 flux density for the same source and S_{avg} is the average of the two flux densities. As expected for a population of non-varying sources the histogram was roughly a gaussian distribution. There were a few outliers which suggest some variability, but that is most likely explainable with the resolution issues.

Figure 17. Difference over Mean Histogram (A98 and A96)

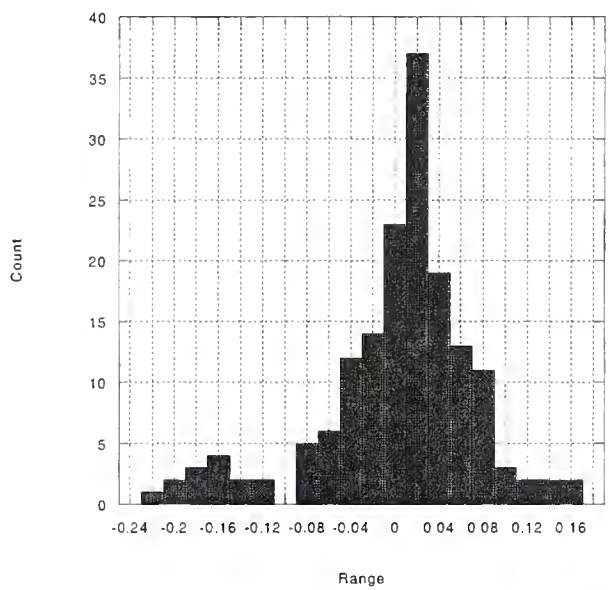

c. Transient criteria and methods

Finally the corrected epoch images could be searched for transient sources. Since we looked field by field for sources, any found on one map and not on the other are suspicious and possibly transient. No sources were found on only the A98 map. Sources listed in Table 6 are those found on B98, but not on A98. Twenty such sources were identified. Each of these sources was examined by remeasuring and consulting data from observations other than the four listed in Table 1. Many were weaker sources that were resolved out on the A98 map. After analysis there were no new convincing transients remaining. Hyman, using a method of subtracting one map from another to check the A98 and AB02 maps for the presence of transients, found none.

Table 6. Sources found on B98, Not A98

Position RA	DEC	Flux Density	ΔS
RA 17 38 16.086	DEC -28 52 27.21	0.105	0.033
RA 17 40 32.991	DEC -28 43 51.46	0.054	0.014
RA 17 41 26.166	DEC -28 53 24.10	0.076	0.016
RA 17 41 29.025	DEC -30 57 27.86	0.221	0.035
RA 17 41 30.832	DEC -29 10 59.03	0.059	0.033
RA 17 41 46.962	DEC -31 25 10.03	0.271	0.101
RA 17 42 21.671	DEC -29 12 52.00	0.122	0.023
RA 17 42 27.441	DEC -29 56 09.71	0.225	0.035
RA 17 42 27.538	DEC -30 09 12.78	0.332	0.031
RA 17 42 54.649	DEC -30 07 04.88	0.076	0.019
RA 17 43 03.057	DEC -28 50 59.34	0.068	0.018
RA 17 43 20.694	DEC -31 10 31.89	0.363	0.098
RA 17 44 25.6955	DEC -29 29 17.665	0.315	0.044
RA 17 44 27.9683	DEC -29 36 03.083	0.088	0.018
RA 17 44 36.1453	DEC -29 35 47.6533	0.252	0.024
RA 17 44 55.541	DEC -29 41 15.24	0.507	0.038
RA 17 45 00.993	DEC -29 28 45.34	0.079	0.019
RA 17 45 26.368	DEC -28 42 38.955	0.229	0.053
RA 17 46 02.031	DEC -28 24 49.99	0.077	0.017
RA 17 46 09.983	DEC -28 23 24.90	0.089	0.014
RA 17 46 27.771	DEC -28 35 53.48	0.210	0.034
RA 17 46 52.6075	DEC -28 07 35.685	0.460	0.031
RA 17 47 44.721	DEC -28 21 36.45	0.752	0.045
RA 17 48 05.222	DEC -28 28 19.39	0.284	0.026
RA 17 50 11.817	DEC -28 53 49.27	0.100	0.014
RA 17 50 14.101	DEC -28 54 29.28	0.128	0.013
RA 17 50 17.528	DEC -28 53 39.29	0.061	0.015
RA 17 50 24.381	DEC -28 53 09.30	0.345	0.028
RA 17 52 29.288	DEC -30 49 05.29	0.271	0.090
RA 17 53 13.905	DEC -28 53 12.10	0.072	0.033
RA 17 42 05.2527	DEC -27 14 54.927	0.164	0.036

Chapter 4 Discussion and Conclusion

One important issue in this research is whether or not the data analyzed are consistent and therefore reliable. The fact that the vast majority of the source measurements from different epochs correspond so well confirms this reliability. The graphs of the flux densities for one map versus another are all linear, needing only an overall correction factor of up to 20% to compare measurement from epoch to epoch. That the slopes of these graphs are not unity is likely due to errors in the data calibration, and is not detrimental to our research since it can be corrected for.

One strange finding in this project was that the 147 source B98 data set has a correction factor of 1.14 and the 102 source B98 data set had no correction factor, a significant difference considering the error in the slope to be 3%. This difference can be attributed to the fact that the list of 147 included more of the smaller and fainter sources that were missed by eye, while the 102 included some of the brighter and more extended sources, which were likely to be measured larger on B98 than A98 because of the resolution difference.

The use of the automated program, SAD, was found to be not as reliable as earlier expected. The somewhat larger scattering of data could cause problems in the correction of the slope of the data set. Ultimately the extraction of the data was just too time consuming for use on the individual epochs. The use of Mike Nord's list of sources made it much easier to measure sources based on their location.

A number of possible transients were found on the B98 map, but no possible transients were found on the A98 map. Of the possible transient sources listed in Table 6, the vast majority can be explained as sources that are extended and are simply resolved

out on the A98 map. The sources were determined to be extended sources by a visual examination of the faded and blending qualities of their edges as well as a comparison of their integrated intensity to their peak intensity.

Similarly the search for variable sources returned a large list of sources with high difference to error ratios. However, even if a source was found to have a significant ratio of difference to error there were factors that might cause this ratio to be high when the source was not truly variable. For example in Table 3 the first source on the list has an R value of over –13. This source was merely a very bright source whose flux density difference was less than 10% of its average flux density, but was so luminous that the difference was still significant compared to the uncertainties and we can not be confident that it is variable since we have systematic uncertainty of that level.

Other factors that caused high R values were irregular shape, particularly weak sources, and resolution differences. About 65% of the sources were thought to have high R values not because they were variable, but because of the resolution differences between maps. Another 30% of the sources were difficult to measure because of either their size or surrounding structure which made the systematic uncertainty higher than the number estimated by IMFIT. The final 5% of the sources were the best variable candidates, however even these had some resolution and background emission issues that cast doubt on their reliability.

The time scale and luminosity of the variables we would be able to detect is also something to take into consideration. If a source appeared for only a short time it might get lost in the map since it is averaged over time to get the final product.

From this small finding we are seeing that the Galactic center actually has relatively few radio transients and variables that pass our detection criteria. Assuming our observations to be a typical representation of Galactic center activity we can calculate the rate of transients by diving those we found by the observing time and the observing area. Including the two transients found by Hyman, we calculate the occurrence of transients brighter than 75mJy and timescales greater than six hours to be no less than $46(^{\circ})^{-2}\,yr^{-1}$. We hope to find variability and transient events at shorter intervals, such as three or four days, with new proposals to the VLA and GMRT.

Appendix A

Table1. All A98, B98 and A96 source measurements (corrected values).

Position (J2000) RA			DEC			A98 Flux (Jy)	ΔS	A96 Flux	ΔS	B98 Flux	ΔS
17	47	20.16	-28	23	3.75	0.165	0.016	0.217	0.027	0.745	0.077
17	47	8.27	-28	34	46.25	0.304	0.036	0.225	0.034	0.353	0.048
17	47	6.21	-28	35	7.57	0.165	0.017	0.265	0.030	0.346	0.027
17	46	51.38	-28	36	7.65	0.083	0.011	0.121	0.009	0.111	0.013
17	45	38.78	-28	28	55.26	0.050	0.014	0.047	0.010	0.058	0.021
17	45	28.85	-28	30	8.72	0.035	0.008	0.037	0.006		
17	45	50.45	-28	49	17.7	0.082	0.014	0.109	0.010	0.446	0.134
17	44	37.12	-28	57	6.23	0.453	0.036	0.654	0.024	0.636	0.023
17	46	51.61	-29	22	12.34	0.017	0.009	0.077	0.018	0.097	0.020
17	44	23.27	-28	14	35.96	0.092	0.011	0.115	0.009	0.111	0.013
17	47	47.42	-30	28	9.86	0.198	0.025	0.179	0.021		
17	47	46.5	-30	28	13.05	0.340	0.031	0.279	0.021		
17	40	32.9	-28	43	49.79	0.069	0.023	0.056	0.019	0.062	0.012
17	46	50.22	-27	41	42.58			0.074	0.015		
17	54	32.85	-29	10	8.57	0.369	0.121	0.351	0.040	0.332	0.040
17	53	55.43	-28	15	50.21	0.366	0.051	0.397	0.040	0.468	0.046
17	47	49.49	-31	23	5.65					0.931	0.052
17	47	45.8	-31	23	31.49					0.306	0.045
17	36	5.4	-28	32	28.07	0.452	0.052	0.395	0.033	0.565	0.033
17	36	21.03	-28	35	50.35	0.551	0.035	0.552	0.031	0.676	0.035
17	36	35.95	-29	0	5.39	0.249	0.053	0.102	0.032	0.395	0.046
17	36	38.78	-29	21	22.7	0.288	0.032	0.319	0.030	0.295	0.031
17	36	40.7	-29	6	54.51	0.203	0.067			0.110	0.031
17	37	24.38	-28	4	29.66	0.297	0.033	0.352	0.032	0.294	0.034
17	37	28.45	-29	7	59.2	0.176	0.030	0.170	0.021	0.145	0.022
17	37	45.47	-29	17	51.71	0.257	0.024	0.305	0.027	0.265	0.021
17	37	57.15	-29	11	36.86	0.148	0.048	0.116	0.030	0.113	0.029
17	38	16.17	-28	52	28.34	0.043	0.017	0.082	0.026	0.137	0.026
17	38	16.53	-29	10	41.17	0.132	0.025	0.152	0.022	0.096	0.017
17	38	23.95	-27	52	53.49	0.130	0.047			0.125	0.052
17	38	27.22	-28	50	0.07			0.049	0.012	0.054	0.020
17	38	49.3	-29	28	47.72	0.089	0.031	0.017	0.011	0.041	0.022
17	39	12.69	-28	46	58.48	0.292	0.021	0.448	0.023		
17	39	26.67	-28	6	14.62	0.230	0.032	0.263	0.024	0.191	0.017
17	39	30.38	-28	43	38.03	0.136	0.022	0.181	0.016	0.280	0.030
17	39	31.98	-28	43	40.02	0.116	0.018	0.148	0.017		
17	39	33.17	-29	41	19.62	0.101	0.029	0.053	0.014	0.051	0.020
17	39	37.92	-28	33	42.3	0.206	0.016	0.299	0.028	0.225	0.018
17	40	0.6	-27	48	15.36	0.464	0.045	0.592	0.042	0.424	0.030
17	40	7.85	-28	42	1.79	0.425	0.061	0.396	0.032	0.317	0.019
17	40	13.42	-28	13	14.02	0.244	0.028	0.218	0.020	0.198	0.016

17	40	7	-30	39	34.03	0.178	0.043	0.148	0.049	0.181	0.040
17	40	20.43	-29	13	41.42	0.058	0.015	0.058	0.017	0.045	0.014
17	40	32.95	-28	33	51.2			0.034	0.015	0.094	0.026
17	40	28.28	-30	43	54.34	0.296	0.044	0.237	0.031	0.226	0.050
17	40	41.61	-28	48	8.31	0.239	0.020	0.329	0.020	0.324	0.015
17	40	54.55	-29	29	47.9	0.193	0.012	0.191	0.011	0.223	0.011
17	41	1.99	-30	32	2.6	0.165	0.047	0.068	0.028	0.098	0.041
17	41	2.91	-30	29	21.84	0.271	0.028	0.349	0.023	0.352	0.029
17	41	11.14	-27	35	15.93	0.124	0.034	0.089	0.022	0.078	0.019
17	41	16.74	-30	23	28.57	0.226	0.035	0.191	0.023	0.175	0.030
17	41	24.01	-28	13	31.28	0.064	0.020	0.072	0.014	0.039	0.010
17	41	20.98	-30	52	42.47	0.234	0.071	0.193	0.042	0.062	0.024
17	41	26.14	-28	53	27.37	0.088	0.021	0.075	0.017	0.091	0.013
17	41	27.26	-29	54	29.42	0.063	0.014	0.072	0.014	0.068	0.014
17	41	28.97	-30	57	30.27			0.162	0.033	0.207	0.037
17	41	37.75	-28	4	36.96	0.333	0.014	0.354	0.016	0.285	0.013
17	41	49.37	-28	43	24.57	0.009	0.005	0.026	0.010	0.018	0.009
17	41	49.6	-29	44	59.72	0.101	0.014	0.149	0.012	0.090	0.010
17	41	53.49	-30	17	52.49	0.130	0.048	0.103	0.022	0.116	0.036
17	42	1.97	-27	13	8.66	0.427	0.035	0.508	0.031	0.440	0.043
17	42	5.27	-27	15	6.54	0.200	0.095	0.125	0.047	0.259	0.046
17	42	2.74	-30	6	40.13	0.431	0.018	0.405	0.015	0.419	0.017
17	42	9.63	-27	22	5.72	0.061	0.023	0.116	0.023	0.075	0.032
17	42	5.05	-30	4	3.19	0.205	0.056	0.153	0.040	0.215	0.023
17	42	12.17	-26	46	17.98					0.065	0.033
17	42	13.27	-29	49	54.38	0.191	0.016	0.169	0.016	0.234	0.020
17	42	18.26	-27	38	25.87	0.089	0.020	0.133	0.018	0.067	0.017
17	42	14.71	-29	50	8.82	0.085	0.022	0.064	0.012		
17	42	21.49	-29	12	53.68				0.005	0.189	0.019
17	42	28.07	-28	2	8.24	0.316	0.013	0.363	0.014	0.292	0.016
17	42	24.99	-30	8	0.9	0.146	0.021	0.153	0.018	0.220	0.023
17	42	28.85	-29	46	53.99	0.013	0.009	0.014	0.008	0.025	0.014
17	42	29.17	-30	6	29.28					0.200	0.029
17	42	43.38	-28	1	19.44	0.024	0.010	0.095	0.024	0.091	0.023
17	42	40.94	-30	22	33.13	0.136	0.025	0.103	0.017	0.083	0.020
17	42	44.02	-29	49	13.33	1.816	0.025	1.849	0.019	1.829	0.020
17	42	48.58	-27	40	36.72	0.085	0.033			0.097	0.050
17	42	48.01	-28	4	31.34	0.140	0.024	0.169	0.024	0.154	0.016
17	42	48.49	-28	25	21.76	0.071	0.015	0.127	0.018	0.108	0.013
17	42	47.07	-29	57	38.74	0.043	0.013	0.027	0.012		
17	42	48.33	-30	9	53.73	0.103	0.023	0.074	0.013	0.069	0.021
17	42	54.49	-30	7	6.28	0.276	0.073	0.040	0.017	0.115	0.018
17	42	59.12	-28	9	36.07	0.090	0.029	0.046	0.011	0.062	0.017
17	43	0.55	-29	50	33.06	0.026	0.010	0.011	0.007	0.010	0.008
17	43	3.13	-28	50	59.94	0.198	0.043	0.108	0.019	0.142	0.014
17	43	5.45	-27	36	2.61	0.506	0.017	0.566	0.016	0.455	0.022
17	43	5.48	-27	49	26.86	0.200	0.018	0.231	0.021	0.234	0.020

17	43	5.68	-29	47	39.15	0.044	0.015	0.109	0.039	0.012	0.008
17	43	15.73	-28	35	10.27	0.036	0.014			0.072	0.014
17	43	14.91	-29	46	47.49	0.092	0.016	0.103	0.012	0.097	0.014
17	43	20.82	-28	16	43.55	0.028	0.013	0.039	0.010	0.043	0.010
17	43	17.86	-30	58	14.71	0.699	0.042	0.555	0.038	0.667	0.042
17	43	22.65	-29	32	2.97	0.013	0.006	0.019	0.010	0.080	0.033
17	43	23.86	-31	13	37.26					0.624	0.165
17	43	28.84	-29	6	45.64	0.187	0.023	0.202	0.019	0.172	0.013
17	43	34.82	-30	1	30.23	0.026	0.012	0.039	0.013	0.043	0.016
17	43	44.55	-29	40	17.71	0.018	0.010	0.008	0.005	0.190	0.040
17	43	50.55	-29	37	12.53	0.256	0.052	0.068	0.014	0.080	0.016
17	43	51.26	-29	54	21.73	0.127	0.050	0.070	0.017	0.218	0.057
17	43	52.15	-31	14	10.68			0.224	0.067	0.265	0.055
17	44	10.84	-29	25	55.17			0.077	0.019	0.595	0.079
17	44	18.68	-30	1	17.81	0.104	0.043	0.047	0.015		
17	44	23.05	-28	15	10.05	0.235	0.017				
17	44	23.12	-30	27	57.03	0.075	0.024	0.035	0.012	0.045	0.027
17	44	23.46	-31	16	33.87			0.493	0.074	0.745	0.067
17	44	27.76	-29	36	8.4	0.097	0.018	0.105	0.011	0.096	0.013
17	44	33.59	-28	18	37.82	0.029	0.012				
17	44	42.57	-28	28	47.69			0.031	0.010		
17	44	48.81	-28	28	11.13	0.062	0.008	0.069	0.008	0.049	0.009
17	44	52.24	-27	47	29.78	0.049	0.021	0.055	0.014	0.085	0.035
17	44	51.58	-30	37	22.4			0.058	0.020	0.065	0.023
17	44	59.39	-29	16	0.73	0.019	0.009	0.017	0.010	0.109	0.028
17	44	59.41	-29	36	59.52	0.058	0.019	0.064	0.021		
17	44	59.7	-29	28	47.11	0.016	0.007	0.208	0.028	0.108	0.021
17	45	3.98	-29	16	35.68					0.338	0.110
17	45	10.9	-27	32	36.72	0.073	0.026	0.082	0.017	0.074	0.014
17	45	13.92	-29	29	24.8	0.033	0.010			0.359	0.098
17	45	39.09	-29	56	12.75	0.036	0.017	0.023	0.010		
17	45	45.15	-28	6	29.32	0.120	0.012	0.131	0.010	0.106	0.013
17	45	47.61	-26	49	6.07			0.303	0.044		
17	45	47.95	-27	55	46.98	0.068	0.013	0.109	0.012	0.094	0.015
17	45	52.53	-28	20	24.57	0.027	0.009	0.050	0.010	0.039	0.011
17	45	56.25	-30	40	21.04	0.057	0.018	0.067	0.017	0.091	0.032
17	46	10.27	-27	57	20.23	0.159	0.071			0.259	0.015
17	46	13.44	-29	48	21.9	0.084	0.033	0.086	0.021	0.085	0.025
17	46	38.73	-27	49	50.6	0.154	0.012	0.181	0.012	0.181	0.018
17	46	50.38	-29	21	39.08	0.027	0.022	0.093	0.031	0.109	0.019
17	46	55.61	-30	42	10.87	0.384	0.034	0.284	0.025	0.258	0.030
17	46	54.47	-28	3	54.52	0.099	0.025	0.092	0.019	0.051	0.020
17	47	7.19	-28	46	2.44	0.081	0.022	0.046	0.011		
17	47	13.4	-30	22	18.2	0.135	0.020	0.116	0.016	0.120	0.017
17	47	12.87	-29	29	16.59	0.171	0.013	0.143	0.009	0.122	0.016
17	47	18.75	-29	27	37.57	0.094	0.021	0.104	0.018	0.059	0.012
17	47	42.68	-29	13	40.15	0.013	0.008				

17	47	56.3	-29	59	34.81	0.099	0.024	0.109	0.018	0.071	0.018
17	47	54.04	-28	3	27.49	0.158	0.012	0.149	0.010	0.136	0.016
17	47	53.6	-27	41	32.69	0.040	0.018	0.058	0.017	0.077	0.038
17	48	1.07	-28	16	3.46	0.008	0.007			0.152	0.028
17	48	5.14	-28	28	22.05					0.330	0.015
17	48	7.08	-28	27	40.25	0.054	0.011	0.078	0.011	0.067	0.012
17	48	13.25	-30	55	31.75	0.646	0.183	0.434	0.096	0.562	0.140
17	48	10.3	-28	56	48.73			0.134	0.026	0.206	0.031
17	48	10.62	-27	45	20.32	0.052	0.022	0.050	0.014	0.094	0.033
17	48	15.59	-30	56	14.04	0.127	0.056	0.169	0.046	0.604	0.124
17	48	26.05	-30	50	27.85	0.097	0.034			0.069	0.044
17	48	27.93	-29	39	6.39					0.485	0.014
17	48	26.86	-27	34	18.56	0.100	0.030				
17	48	28.89	-28	33	12.84			0.058	0.012	0.064	0.013
17	48	39.19	-29	32	1.8	0.032	0.010	0.019	0.006		
17	48	45.74	-29	7	35.22	0.066	0.016	0.078	0.019	0.133	0.035
17	48	52.97	-29	26	54.74	0.047	0.009	0.050	0.006	0.051	0.012
17	48	51.65	-27	39	12.58	0.059	0.014	0.087	0.019	0.082	0.032
17	49	2.09	-29	55	7.46	0.187	0.016	0.212	0.015	0.175	0.011
17	49	2.28	-29	12	22.35	0.080	0.032	0.043	0.014	0.065	0.019
17	49	8.44	-30	27	20.01	0.221	0.057	0.056	0.016	1.025	0.137
17	49	9.8	-30	45	5.05	0.388	0.033	0.263	0.028	0.378	0.036
17	49	7.24	-29	23	36.04	0.520	0.016	0.652	0.021	0.783	0.011
17	49	13.48	-30	2	32.71	0.026	0.012	0.065	0.015	0.042	0.017
17	49	14.6	-28	15	37.12	0.031	0.011	0.032	0.013	0.038	0.012
17	49	19.3	-27	21	12.31	0.094	0.037	0.193	0.059	0.276	0.091
17	49	28.11	-30	35	16.09	0.145	0.030	0.089	0.025	0.128	0.030
17	49	26.93	-28	15	42.88	0.067	0.019	0.065	0.014	0.079	0.022
17	49	30.39	-28	53	3.36	0.027	0.014	0.040	0.012		
17	49	31.97	-29	34	9.37	0.139	0.028	0.098	0.015	0.120	0.018
17	49	32.83	-27	50	15.84	0.053	0.022	0.039	0.010	0.059	0.021
17	49	49.09	-28	55	4.57	0.056	0.013	0.054	0.009		
17	49	51.62	-29	52	35.27	0.059	0.021	0.060	0.018	0.044	0.014
17	49	58.17	-29	25	20.27	0.197	0.045	0.157	0.022	0.132	0.016
17	50	0.29	-27	54	0.68	0.031	0.016	0.550	0.090	0.157	0.019
17	50	2.27	-27	48	6.07	0.168	0.028	0.126	0.019	0.157	0.027
17	50	6.58	-29	22	29.65	0.148	0.017	0.164	0.017	0.141	0.011
17	50	8.51	-28	52	39.58	0.125	0.012	0.143	0.009	0.128	0.009
17	50	12.25	-28	53	41.33	0.034	0.018			0.209	0.023
17	50	14.17	-28	54	23.54	0.307	0.052	0.183	0.027	0.188	0.028
17	50	24.18	-28	53	2.76					0.436	0.036
17	50	25.45	-27	55	39.93	0.191	0.020	0.227	0.018	0.187	0.018
17	50	30.87	-28	48	31.66	0.124	0.012	0.131	0.010	0.136	0.010
17	50	38.42	-29	28	20.81	0.063	0.022	0.080	0.013	0.063	0.014
17	50	33.65	-27	2	29.14					0.057	0.037
17	50	43.35	-29	37	58.05	0.039	0.010	0.054	0.014	0.053	0.017
17	50	51.36	-29	23	43.34	0.150	0.014	0.135	0.009	0.131	0.013

17	50	51.54	-29	3	15.38	0.073	0.011	0.078	0.011	0.086	0.012
17	51	6.73	-30	22	15.1	0.146	0.036	0.152	0.042	0.085	0.032
17	51	4.63	-28	36	23.87			0.058	0.016	0.038	0.016
17	51	14.03	-29	49	37.94	0.056	0.015	0.059	0.013	0.098	0.023
17	51	12.56	-27	37	17.55	0.101	0.038	0.119	0.032		
17	51	21.1	-30	13	46.58	0.300	0.055	0.207	0.044	0.162	0.025
17	51	20.48	-29	33	29.84	0.069	0.013	0.061	0.011	0.053	0.011
17	51	21.34	-28	41	29.45	0.038	0.011	0.075	0.012	0.061	0.019
17	52	17.09	-30	7	8.49	0.217	0.031	0.205	0.022	0.197	0.032
17	52	14.83	-28	43	20.73	0.086	0.018	0.102	0.021	0.068	0.022
17	52	17.98	-28	5	31.19	0.213	0.035	0.172	0.027	0.129	0.026
17	52	22.73	-28	37	36.23	1.041	0.028	1.030	0.023	1.173	0.033
17	52	30.89	-30	1	4.21	0.900	0.035	0.813	0.031	0.860	0.031
17	52	33.07	-29	56	42.34	0.559	0.032	0.545	0.023	0.561	0.027
17	52	39.95	-29	56	50.12	0.248	0.031	0.193	0.023	0.223	0.032
17	52	44.05	-30	49	1.55			0.212	0.038	0.250	0.039
17	52	51.75	-30	9	22.94	0.166	0.051	0.154	0.032	0.221	0.051
17	52	56.71	-29	30	43.2	0.137	0.019	0.103	0.016	0.139	0.019
17	52	55.56	-28	57	41.62	0.084	0.026	0.136	0.027	0.074	0.018
17	53	1.19	-29	20	42.74	0.032	0.021			0.050	0.014
17	52	58.7	-28	6	36.98	1.156	0.035	1.242	0.029	1.300	0.030
17	53	5.41	-29	3	26.93	0.192	0.025	0.161	0.016	0.195	0.022
17	53	13.61	-28	53	9.06	0.119	0.039	0.053	0.019	0.108	0.022
17	53	33.68	-28	35	36.56	0.335	0.031	0.386	0.027	0.372	0.022
17	53	40.53	-29	2	53.9			0.078	0.025	0.123	0.041
17	53	48.5	-27	55	15.77	0.152	0.046	0.115	0.022	0.108	0.044
17	53	48.9	-27	56	58.81	0.203	0.064	0.206	0.047	0.197	0.045
17	53	59.19	-28	17	18.59	0.199	0.038	0.254	0.043	0.209	0.031
17	54	12.79	-28	54	16.38	0.165	0.045	0.126	0.033	0.057	0.018
17	54	49.22	-29	54	36.26			0.085	0.031	0.176	0.055
17	55	32.11	-28	59	15.37			0.118	0.028	0.110	0.038

Appendix B

Table 1. All AB02 Source measurements (corrected)

Position (J2000) RA			DEC			AB02 Flux	ΔS
17	54	12.79	-28	54	16.38	0.274	0.029
17	53	59.19	-28	17	18.59	0.244	0.034
17	53	5.41	-29	3	26.93	0.226	0.027
17	53	48.9	-27	56	58.81	0.100	0.029
17	53	48.5	-27	55	15.77	0.247	0.051
17	53	33.68	-28	35	36.56	0.341	0.026
17	53	13.61	-28	53	9.06	0.048	0.013
17	52	58.7	-28	6	36.98	1.225	0.042
17	52	56.71	-29	30	43.2	0.127	0.023
17	52	55.56	-28	57	41.62	0.146	0.036
17	52	51.75	-30	9	22.94	0.135	0.038
17	52	39.95	-29	56	50.12	0.196	0.023
17	52	33.07	-29	56	42.34	0.525	0.028
17	52	30.89	-30	1	4.21	0.867	0.033
17	52	22.73	-28	37	36.23	1.106	0.032
17	52	17.98	-28	5	31.19	0.182	0.032
17	52	17.09	-30	7	8.49	0.213	0.024
17	52	14.83	-28	43	20.73	0.071	0.016
17	51	6.73	-30	22	15.1	0.444	0.056
17	51	21.34	-28	41	29.45	0.090	0.024
17	51	21.1	-30	13	46.58	0.376	0.072
17	51	20.48	-29	33	29.84	0.066	0.011
17	51	14.03	-29	49	37.94	0.085	0.022
17	50	8.51	-28	52	39.58	0.165	0.013
17	50	6.58	-29	22	29.65	0.126	0.016
17	50	51.54	-29	3	15.38	0.106	0.013
17	50	51.36	-29	23	43.34	0.157	0.013
17	50	43.35	-29	37	58.05	0.011	0.007
17	50	38.42	-29	28	20.81	0.062	0.011
17	50	30.87	-28	48	31.66	0.121	0.012
17	50	25.45	-27	55	39.93	0.234	0.019
17	50	2.27	-27	48	6.07	0.178	0.019
17	50	14.17	-28	54	23.54	0.174	0.025
17	50	0.29	-27	54	0.68	0.207	0.049
17	49	9.8	-30	45	5.05	0.442	0.035
17	49	8.44	-30	27	20.01	0.095	0.033
17	49	58.17	-29	25	20.27	0.120	0.018
17	49	51.62	-29	52	35.27	0.107	0.033
17	49	49.09	-28	55	4.57	0.050	0.020

17	49	32.83	-27	50	15.84	0.052	0.020
17	49	31.97	-29	34	9.37	0.102	0.015
17	49	30.39	-28	53	3.36	0.052	0.020
17	49	26.93	-28	15	42.88	0.072	0.014
17	49	2.09	-29	55	7.46	0.194	0.016
17	49	19.3	-27	21	12.31	0.123	0.034
17	49	14.6	-28	15	37.12	0.123	0.021
17	49	13.48	-30	2	32.71	0.028	0.012
17	48	7.08	-28	27	40.25	0.089	0.014
17	48	52.97	-29	26	54.74	0.081	0.021
17	48	51.65	-27	39	12.58	0.091	0.024
17	48	45.74	-29	7	35.22	0.037	0.007
17	48	39.19	-29	32	1.8	0.022	0.009
17	48	15.59	-30	56	14.04	0.121	0.055
17	48	13.25	-30	55	31.75	0.501	0.120
17	48	10.62	-27	45	20.32	0.096	0.037
17	47	7.19	-28	46	2.44	0.028	0.021
17	47	56.3	-29	59	34.81	0.183	0.057
17	47	54.04	-28	3	27.49	0.185	0.019
17	47	53.6	-27	41	32.69	0.166	0.041
17	47	13.4	-30	22	18.2	0.164	0.017
17	47	12.87	-29	29	16.59	0.176	0.028
17	46	55.61	-30	42	10.87	0.348	0.035
17	46	50.38	-29	21	39.08	0.113	0.025
17	46	38.73	-27	49	50.6	0.216	0.019
17	45	56.25	-30	40	21.04	0.202	0.052
17	45	52.53	-28	20	24.57	0.056	0.013
17	45	47.95	-27	55	46.98	0.101	0.011
17	45	45.15	-28	6	29.32	0.118	0.015
17	44	59.39	-29	16	0.73	0.171	0.029
17	44	52.24	-27	47	29.78	0.095	0.027
17	44	48.81	-28	28	11.13	0.080	0.015
17	44	27.76	-29	36	8.4	0.130	0.023
17	43	5.48	-27	49	26.86	0.293	0.021
17	43	5.45	-27	36	2.61	0.635	0.023
17	43	51.26	-29	54	21.73	0.146	0.028
17	43	50.55	-29	37	12.53	0.075	0.015
17	43	44.55	-29	40	17.71	0.019	0.014
17	43	3.13	-28	50	59.94	0.137	0.037
17	43	28.84	-29	6	45.64	0.230	0.015
17	43	17.86	-30	58	14.71	0.608	0.053
17	43	14.91	-29	46	47.49	0.089	0.012
17	42	59.12	-28	9	36.07	0.073	0.010
17	42	48.49	-28	25	21.76	0.144	0.016
17	42	48.33	-30	9	53.73	0.103	0.019

17	42	48.01	-28	4	31.34	0.205	0.032
17	42	44.02	-29	49	13.33	1.913	0.022
17	42	40.94	-30	22	33.13	0.113	0.027
17	42	28.07	-28	2	8.24	0.345	0.022
17	42	2.74	-30	6	40.13	0.399	0.020
17	42	1.97	-27	13	8.66	0.563	0.040
17	42	18.26	-27	38	25.87	0.105	0.015
17	42	14.71	-29	50	8.82	0.108	0.027
17	42	13.27	-29	49	54.38	0.201	0.014
17	41	53.49	-30	17	52.49	0.051	0.022
17	41	49.6	-29	44	59.72	0.141	0.016
17	41	37.75	-28	4	36.96	0.338	0.024
17	41	2.91	-30	29	21.84	0.341	0.041
17	41	27.26	-29	54	29.42	0.080	0.014
17	41	26.14	-28	53	27.37	0.138	0.021
17	41	24.01	-28	13	31.28	0.078	0.022
17	41	20.98	-30	52	42.47	0.154	0.036
17	41	16.74	-30	23	28.57	0.158	0.020
17	41	11.14	-27	35	15.93	0.266	0.045
17	40	7	-30	39	34.03	0.108	0.033
17	40	7.85	-28	42	1.79	0.492	0.030
17	40	54.55	-29	29	47.9	0.204	0.009
17	40	41.61	-28	48	8.31	0.325	0.027
17	40	32.9	-28	43	49.79	0.057	0.016
17	40	28.28	-30	43	54.34	0.253	0.037
17	40	20.43	-29	13	41.42	0.057	0.017
17	40	13.42	-28	13	14.02	0.234	0.021
17	40	0.6	-27	48	15.36	0.606	0.050
17	39	26.67	-28	6	14.62	0.347	0.027
17	38	49.3	-29	28	47.72	0.010	0.010
17	38	23.95	-27	52	53.49	0.128	0.049
17	38	16.53	-29	10	41.17	0.122	0.022
17	38	16.17	-28	52	28.34	0.276	0.056
17	37	57.15	-29	11	36.86	0.114	0.024
17	37	45.47	-29	17	51.71	0.260	0.024
17	37	28.45	-29	7	59.2	0.205	0.022
17	37	24.38	-28	4	29.66	0.410	0.041
17	36	38.78	-29	21	22.7	0.326	0.026
17	36	35.95	-29	0	5.39	0.339	0.073
17	36	21.03	-28	35	50.35	0.641	0.034
17	47	6.21	-28	35	7.57	0.237	0.016
17	47	20.16	-28	23	3.75	0.225	0.032

References

Anantharamaiah, K. R., Pedlar, A., Elkers R.D., & Goss, W.M. 1991, MNRAS, 249, 262

Bally, J., &Yusef-Zadeh, F. 1989, ApJ, 194, 265

Davies, R.D., et al. Letter: "Transient radio source near the galactic center" Nature **261** (1976): 476-478.

Fender, R.P., and E. Kuulkers. "On the peak radio and X-ray emission from neutron star and black hole candidate X-ray transients" Mon. Not. R. Astron. Soc. **324** (2001): 923-930.

Gray, A. D., Cran, L.E., Ekers R.D., &Goss W.M. 1991, Nature, 353, 237

Hyman, Scott D., et al. "Low-Frequency Radio Transients in the Galactic Center" The Astronomical Journal **123** (2002): 1497-1501.

In 't Zand, Jean. "X-Ray Transients in the Galactic Center Region" Invited paper to the 4th INTEGRAL workshop "Exploring the gamma-ray universe", Alicante (Spain), Sep. 4-8, 2000.

King, A.R. "The Population of Faint Transients in the Galactic Center" Mon. Not. R. Astron. Soc. 2001.

Kraus, John D. Radio Astronomy 2nd edition. Ohio: Cygnus-Quasar Books, 1996.

LaRosa, T.N., et al. "A Wide-Field 90 Centimeter VLA Image of the Galactic Center Region" The Astonomical Journal **119** (2000): 207-240.

Morris, M., & Yusef-Zadeh, F. 1985, The Astronomical Journal, 90, 2511

Reber 1940 Astrophysics Journal, Reber 1940 Proc. IRE.

Zeilik, Michael., and Stephen A. Gregory. Introductory Astronomy and Astrophysics 4th edition. Fort Worth: Saunders College Publishing, 1998.

Zhao, Jun-Hui, et al. "A Transient Radio Source near the Center of the Milky Way Galaxy" Science **255** (1992): 1538-1543.

2329 1382 11
02/24/04 MAB